PAPER

Check for updates

Investigating the potent antibacterial, antibiofilm, antidiabetic, and antioxidant activities of biosynthesized iron oxide nanoparticles: recyclable catalyst for ammoxidation of aromatic aldehydes

Asit Kumar Das, [iD] *[a] Arindam Misra,[a] Md Sattar Ali,[a] Md Sultan Saikh,[a] Subhendu Dhibar,[b] Kalyan Kumar Banerjee,[c] Gourav Ghatak,[d] Dasarath Mal, [iD] [e] Manik Shit[f] and Smritikana Biswas*[d]

An economically efficient and operationally simple method was developed for synthesizing Fe_3O_4 nanoparticles using the aqueous peel extract of *Punica granatum* L. fruit. The biosynthesized Fe_3O_4@PPE nanoparticles were characterised using different analytical techniques, such as UV-visible spectroscopy, Fourier transform infrared spectroscopy (FTIR), X-ray diffraction (XRD) analysis, scanning electron microscopy (SEM), energy-dispersive X-ray analysis (EDAX), elemental mapping analysis, transmission electron microscopy (TEM), dynamic light scattering (DLS) and zeta potential analysis, which confirmed their outstanding morphology and stability. The synthesized nanoparticles were investigated as a potent source of antimicrobials towards methicillin-resistant *Staphylococcus aureus* (Gram-positive MRSA1 and MRSA2) and *Escherichia coli* (Gram-negative). Moreover, the biosynthesized Fe_3O_4@PPE NPs were effective in inhibiting chronic infections by decreasing the biofilm formation. The biosynthesized Fe_3O_4@PPE NPs demonstrated anti-diabetic properties by inhibiting amylase activity (50.89% alpha-amylase inhibition at 400 μg mL^{-1}) and scavenging ROS (78.5% at 200 μg mL^{-1}), highlighting their anti-oxidant activity. Moreover, the catalytic efficiency of the biosynthesized Fe_3O_4@PPE NPs was explored for the ammoxidation of aromatic aldehydes to aryl nitriles under an O_2 atmosphere. Notably, the catalyst was recycled and used for five consecutive cycles, and its good catalytic reactivity was maintained. This study provides a green synthetic route for nitriles from easily accessible aldehydes and ammonia using a cost-effective catalyst in the presence of atmospheric O_2 as an eco-friendly oxidant.

1. Introduction

Metal oxide nanoparticles are attractive candidates for the scientific community because of their quantum size, electron-confining ability, remarkable surface-to-volume ratio, high catalytic activity, and good selectivity compared with their corresponding bulk material.[1] Metal oxide nanoparticles have been synthesized using a variety of physio-chemical techniques, including ion sputtering,[2] hydrothermal,[3] reverse micelle,[4] sol–gel,[5] co-precipitation,[6] polymers,[7] metal–organic frameworks[8] in the last few years. Although the reported methods have their merits, most of them employ hazardous reagents, expensive

chemicals, high-temperature calcination, and toxic nonpolar solvents, which show adverse impacts on the environment from a sustainability perspective. Recently, plant extract-mediated synthesis of metal oxide nanoparticles has been considered an economically efficient and environmentally benign alternative to conventional physical and chemical methods of production of metal oxide nanoparticles.[9] Moreover, metal oxide nanoparticles synthesized by biogenic approaches have been reported to exhibit no toxicity in contrast to nanoparticles produced by physio-chemical methods. Recently, the use of metal oxide nanoparticles has increased significantly in clinical and industrial fields.[10] It is very essential to protect medical and surgical devices and materials for implantation from any bacterial growth to reduce disease transmission.[11] However, resistance to several antimicrobial agents and biofilm formation on medical devices remain as major problems.[12] The presence of methicillin-resistant *Staphylococcus aureus* has now increased all over the world. Biofilms are essential for their survival in a reservoir for a long time, which cause chronic infection.[13–15] To date, several studies have synthesised new

[a]Department of Chemistry, Murshidabad University, Berhampore, 742101, India. E-mail: akdche@msduniv.ac.in

[b]Department of Physics, Indian Institute of Technology Patna, Bihar, 801106, India

[c]Department of Physics, Jadavpur University, Kolkata, 700032, India

[d]Department of Physiology, Murshidabad University, Berhampore, 742101, India. E-mail: physio.smriti2005@gmail.com

[e]Department of Chemistry, Vijaygarh Jyotish Ray College, Kolkata, 700032, India

[f]Department of Chemistry, Narajole Raj College, Paschim Medinipur, 721211, India

antimicrobials with novel strategies for killing microorganisms, such as iron oxide nanoparticles with bactericidal and fungicidal activity.[16–18] Several researchers have shown the anti-biofilm activity of such synthesized iron oxide nanoparticles.[16–19]

In this context, the present study focused on the biogenic synthesis of Fe_3O_4 nanoparticles using *Punica granatum* L. fruit peel extract (PPE). Agricultural residues obtained from fruits are attracting significant attention because of their low cost, low toxicity, and high abundance. Pomegranate peels contain a significant number of phenolic compounds, which are widely recognised as a natural source of antioxidants (Fig. 1).[20] As a result, pomegranate fruit peels were used in the green synthesis of metal oxide nanoparticles in an aqueous phase due to the general significance of using natural, renewable, and low-cost materials, thereby avoiding the effects of harmful reagents and hazardous solvents. Moreover, in this work the biosynthesized Fe_3O_4@PPE NPs were investigated for their anti-oxidant and anti-diabetic properties, antibacterial properties against *E. coli* and *S. aureus*, and role against the biofilm formation by *Staphylococcus aureus* strains (MRSA1 and MRSA2).

In developing advanced synthetic approaches, "green chemistry" has been regarded as a crucial factor for centuries; it is considered that the synthetic strategies[21–25] without a green procedure will become incompetent with time. In the field of modern organic synthesis, nitriles and their derivatives are valuable intermediates for the synthesis of polymers, materials, pigments, dyes, pharmaceuticals, and natural products.[26] Furthermore, nitriles are a prevalent pharmacophore in many commercially available drugs, including Letrozole® (used for breast cancer treatment), Fadrozole® (used for oncolytic drug), Citalopram® (used for antidepressant drug), Periciazine® (used

for anti-psychotic drug), Etravirine® (used for anti-HIV), and Bicalutamide® (used for prostate and breast cancer treatments).[27] Traditional approaches for synthesizing nitriles involve the Sandmeyer reaction[28] and the Rosenmund–von Braun reaction.[29] However, these methods require extremely toxic cyanides and harsh reaction conditions and produce significant amounts of waste in the environment, which is highly undesirable from a sustainability perspective. Moreover, several reports on the synthesis of nitriles, such as oxidative rearrangement of alkenes,[30] cyanation of aryl halides,[31] hydro-cyanation of alkenes,[32] methyl arenes,[33] benzyl or allyl halides,[34] and oxidative transformation of aldehydes[35] have been developed in the last few years. Some reported methods have serious limitations, such as the requirement for capricious ligands, high temperatures, or harmful reagents, low tolerance to functional groups, low atom economy or harsh reaction conditions. Therefore, it is essential to develop atom-economic and greener routes[36,37] to nitriles. Catalytic ammoxidation of aromatic aldehydes to nitriles is an important class of organic transformation because of its economic viability, synthetic utility, and environmental efficiency.[38] The ammoxidation method requires ammonia and oxygen, thereby circumventing the use of hazardous reagents and meeting the basic criteria of green chemistry principles through the utilization of renewable feedstocks with high atom-economy and good selectivity.[39–41] Remarkably, Fe-based catalysts have been extensively explored because of their high abundance, low toxicity and cost-effectiveness. Therefore, Fe-based catalysts can be ideal candidates for replacing some existing precious transition metal catalysts. Due to these advantages, we have developed the catalytic ammoxidation of aromatic aldehydes to aryl nitriles using bio-based iron oxide nanoparticles (Fe_3O_4@PPE) as an efficient recyclable catalyst in the presence of aqueous NH_3 as
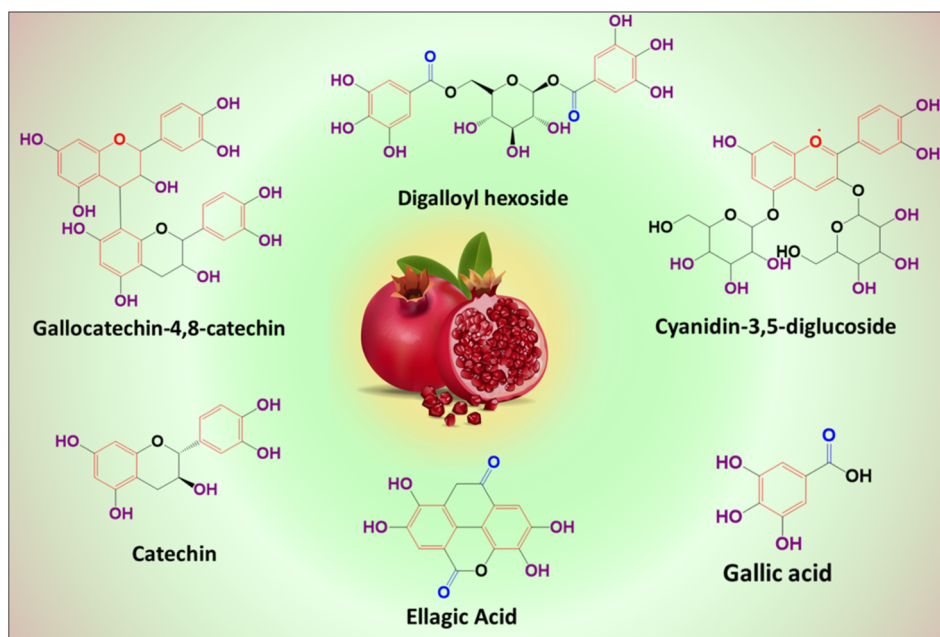

Fig. 1 Different types of secondary metabolites involved in the biosynthesis of metallic nanoparticles from pomegranate peels.

the source of nitrogen and atmospheric O_2 as an eco-friendly oxidant. The present work establishes an eco-friendly route for synthesizing Fe_3O_4 nanoparticles using agricultural waste, demonstrating their multiple functionality as antimicrobial agents (effective against methicillin-resistant *Staphylococcus aureus* and *Escherichia coli*), therapeutic substances (exhibiting antioxidant and anti-diabetic activities), and recyclable catalysts for the synthesis of pharmaceutically important nitriles using atmospheric oxygen. This study also develops a sustainable platform that combines waste valorisation, nanotechnology development, and eco-friendly organic synthesis with potential applications in healthcare and pharmaceutical production.

2.   Experimental section

2.1.   Materials and reagents

Ferrous sulphate heptahydrate ($FeSO_4 \cdot 7H_2O$) was purchased from Sigma-Aldrich, India. The peel extract used in the study was obtained from *Punica granatum* L. fruit that was collected from Berhampore, Murshidabad, India. All preparations were carried out with double-deionized water.

2.2.   Preparation of peel extract

Punica granatum L. fruits (commonly called "pomegranate") were collected from Berhampore, Murshidabad, India. The peels were separated from the fruits and washed several times with double-deionized water to remove unwanted dust materials. The peels were then diced into fine pieces (approximately 1 cm) and dried for seven days at room temperature. The extract was prepared using the dried peels. To prepare the extract, 10 g of *Punica granatum* L. dried fruit peels were weighed and added to 100 mL of double-deionized water in a 250 mL Erlenmeyer flask. The mixture was then boiled for 30 minutes with continuous stirring to obtain the aqueous extract. The yellow plant extract was filtered through Whatman No. 41 filter paper and stored at 4 °C for further investigations.

2.3.   Synthesis of Fe_3O_4@PPE NPs from aqueous peel extract

Fe_3O_4@PPE nanoparticles have been synthesized using natural resources as replacements for harmful chemicals, advancing green practices and reducing superfluous waste generation (Fig. 2). For the synthesis of Fe_3O_4@PPE NPs, in a 25 mL Erlenmeyer flask, 10 mL of the pomegranate fruit peel aqueous extract was mixed with 0.1 g of ferrous sulphate heptahydrate ($FeSO_4 \cdot 7H_2O$) at room temperature in an ambient atmosphere. The immediate appearance of a black colour in the solution indicated the formation of iron oxide nanoparticles. The NPs were centrifuged at 10 000 rpm and washed several times with double-deionized water and ethanol to eliminate dust particles. The obtained black product was then dried in an oven.

2.4.   General experimental procedure for the ammoxidation of aromatic aldehydes

To a stirred suspension of the appropriate aromatic aldehyde (1.0 mmol) in EtOH (4 mL), Fe_3O_4@PPE (40 mg) was added, followed by 800 μL of $NH_3 \cdot H_2O$ (Table 1). The reaction mixture was stirred at 60 °C in an oxygen atmosphere for 24 hours to complete the reaction. Thin-layer chromatography (TLC) was
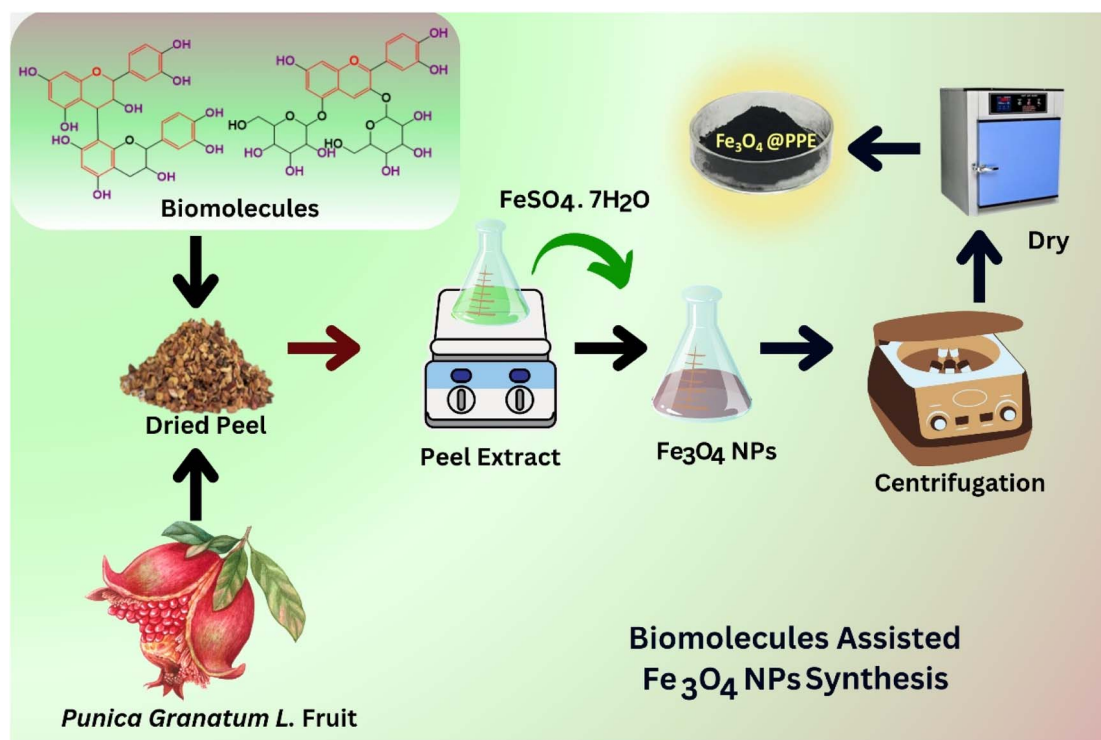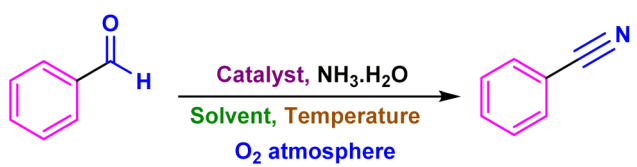

Fig. 2 Schematic of the green synthesis of Fe_3O_4@PPE NPs using the aqueous peel extract of *Punica granatum* L. fruit.

Table 1 Screening of reaction conditions for the ammoxidation of aromatic aldehydes[a]

Entry	Catalyst (wt%)	$NH_3 \cdot H_2O$ (μL)	O_2	Solvent	Temp. (°C)	Time (h)	Yield[b] (%)
1	—	600	+	EtOH	40	20	—
2	Fe_3O_4@PPE (2.4)	700	+	EtOH	40	20	47
3	Fe_3O_4@PPE (3.2)	800	+	EtOH	60	24	72
4	Fe_3O_4@PPE (4.2)	800	+	EtOH	60	24	91
5	Fe_3O_4@PPE (5.2)	800	+	EtOH	60	24	90
6	Fe_3O_4@PPE (4.2)	800	−	EtOH	60	24	—
7	Fe_3O_4@PPE (4.2)	800	+	EtOH	80	24	68
8	Fe_3O_4@PPE (4.2)	800	+	H_2O	60	24	80
9	Fe_3O_4@PPE (4.2)	800	+	n-hexane	60	24	33
10	Fe_3O_4@PPE (4.2)	800	+	CH_3CN	60	24	51
11	Fe_3O_4@PPE (4.2)	800	+	DMF	60	24	48
12	Fe_3O_4@PPE (4.2)	800	+	DMSO	60	24	69

[a] Reaction conditions: benzaldehyde (1.0 mmol), solvent (4 mL), catalyst and temperature (as indicated), under O_2 atmosphere. [b] Yield of isolated product. (+)/(−) indicates the reaction was carried out in the presence/absence of O_2 atmosphere, respectively.

used for monitoring the progress of the reaction. Upon completion of the reaction, ethyl acetate (3×3 mL) was used to extract the crude product. The organic layer was dried with anhydrous sodium sulphate to remove remaining water. The solvent was removed under reduced pressure to afford the crude products. Finally, the crude product was purified by filtration chromatography on a short column of silica gel with ethyl acetate–hexane as eluent. The catalyst was recovered from the aqueous part by centrifugation (15 000 rpm), and the isolated catalyst was washed with EtOH several times and dried for further use in the next catalytic reaction.

2.5. Characterization of Fe_3O_4@PPE nanoparticles

A Shimadzu FTIR-8400S spectrophotometer was used to record Fourier transform infrared (FTIR) spectra. XRD data of the powdered sample were measured in transmission mode using a Bruker D2 Phaser X-ray diffractometer (30 kV, 10 mA) and Cu-Kα ($\lambda = 1.5406$ Å) radiation. A Zeiss (Gemini) scanning electron microscope was used to record FESEM images of the samples. Energy dispersive X-ray spectroscopy (EDX) was carried out using a Hitachi S3400N instrument. Transmission electron microscopic images were obtained using a JEOL 2010 TEM operating at 200 kV. A dynamic light scattering (DLS) system (Malvern Zetasizer Nano) was used to investigate the particle size distribution and determine the zeta potential.

2.6. Bacterial strains used for the study

Methicillin-resistant *Staphylococcus aureus* (MRSA1 and MRSA2) and *Escherichia coli* were used in the present study. Methicillin-resistant *Staphylococcus aureus* strains used in this study were laboratory strains isolated from post-operative wounds, as

previously reported.[42] All of the strains were cultured on LB agar plates at 37 °C.

2.7. Antibacterial activity of the biosynthesized Fe_3O_4@PPE NPs

The antimicrobial activity of biosynthesized Fe_3O_4@PPE NPs was tested against *Staphylococcus aureus* (MRSA1 and MRSA2) and *Escherichia coli* using the agar well diffusion method. Diluted cultures (0.1 mL) of *Staphylococcus aureus* (MRSA1 and MRSA2) and *Escherichia coli* were spread on mannital salt (MRSA1) and Mueller–Hinton agar plates (MRSA1, MRSA2 and *E. coli*), respectively. Fe_3O_4@PPE NPs (40 μL) were added to the well made in the plate, and the plates were incubated at 37 °C for 24 to 48 h. The zone of inhibition was determined to study the antimicrobial activity of the NPs towards the target strains. The antimicrobial activity assays were performed in triplicate together with controls.[32,33] Distilled water was used as a negative control.

2.8. Concentration-dependent antibacterial activity

The effect different concentrations of Fe_3O_4@PPE NPs (250, 500, 750, and 1000 μg mL^{-1}) on the antibacterial activity against the target bacteria was studied using the agar well diffusion method.[43,44]

2.9. Minimum inhibitory concentration and minimum bactericidal concentration (MIC and MBC) determination

The MIC of the Fe_3O_4@PPE NPs for each strain was determined. The nanoparticle solutions were diluted to final concentrations of 1000, 500, 300, 250, 200, 150, 125, 100, and 60 μg mL^{-1} 100 μL

of each bacterial strain (3.5×10^4 CFU mL^{-1}) was spread on the respective Mueller–Hinton agar plates, and samples of each dilution of Fe$_3$O$_4$@PPE NPs (40 µL) were administered to the wells in the plates. The plates were then incubated at 37 °C for 24 to 48 h. The highest dilution or lowest concentration of the nanoparticles producing an inhibitory zone after 24 h was considered the MIC, and the concentration at which all bacterial cells were killed was regarded as the minimum bactericidal concentration (MBC).[45]

2.10. Study of the effect of the biosynthesized Fe$_3$O$_4$@PPE NPs on the biofilm formation by MRSA1 and MRSA2

The effect of the biosynthesized Fe$_3$O$_4$@PPE NPs on biofilm formation by MRSA1 and MRSA2 was studied using the standard protocol with further modification.[46] Tryptone soy broth and 0.25% glucose were used to culture MRSA1 and MRSA2, and 50 µL of Fe$_3$O$_4$@PPE NPs was added to generate the test samples. Similarly, the target strains were grown in the absence of Fe$_3$O$_4$@PPE NPs as the control group. A blank group (containing only TSB and glucose) was also prepared. Each strain (40 µL) was inoculated in 5 mL TSB in test tubes, and after incubating for 6 h, 500 µL of this bacterial culture was transferred to the respective test tubes. All the cultures were then kept for 18 h at 37 °C. Phosphate-buffered saline (500 µL) was used to clean the test tubes gently, three times. All the test tubes were allowed to dry. To stain the biofilm, 0.1% safranin was administered to the test tubes and kept for 30 seconds. All the test tubes were then rinsed, and absorbance was measured at 490 nm with a spectrophotometer (Systronics, India). This experiment was conducted thrice.

2.11. Alpha amylase inhibition by the biosynthesized Fe$_3$O$_4$@PPE NPs

Inhibition of alpha-amylase activity by the Fe$_3$O$_4$@PPE NPs was tested *in vitro*. Alpha amylase (25 µL), 10 µL sample, 40 µL solution of starch and 15 µL PBS (phosphate-buffered saline) were mixed stepwise. This composition was kept for half an hour in an incubator at 50 °C with supplementation of 20 µL HCl (1 M) and 90 µL of iodine solution. DMSO and acarbose were used as negative and positive controls, respectively.[47] Absorbance was measured at 540 nm using a spectrophotometer (UV-vis dual beam spectrophotometer, Systronics).

$$\text{Enzyme inhibition (\%)} = \frac{(\text{absorption of sample} - \text{absorption of negative control}) \times 100}{(\text{absorption of blank} - \text{absorption of negative control})}$$

OD_S = optical density of the sample; OD_N = optical density of the negative control; OD_B = optical density of the blank.

2.12. Antioxidant capacities of the biosynthesized Fe$_3$O$_4$@PPE NPs

Evaluation of the scavenging activity of Fe$_3$O$_4$@PPE NPs was made with a methanolic DPPH solution (1 mM). Different concentrations of Fe$_3$O$_4$@PPE NPs were used (1, 2, 5, 15, 25, 50, 100, and 200 µg mL^{-1}). After the addition of a methanolic

solution of DPPH to the test samples, all the reaction mixtures were kept for 30 min at room temperature. Absorbance was measured at 517 nm against the respective blank solution with a dual-beam UV spectrophotometer (Systronics, India). The analyses were performed in triplicate, and the DPPH radical scavenging activity (%) was calculated using the following equation:

$$\text{Percentage of scavenging activity} = \frac{A_{\text{control}} - A_{\text{sample}}}{A_{\text{control}}} \times 100$$

The total reducing power (TRP) of the Fe$_3$O$_4$@PPE NPs was also studied using the potassium ferricyanide protocol.[48] Ascorbic acid and DMSO were used as positive and negative controls, respectively. The absorbance was measured at 630 nm. The reduction power was calculated in terms of ascorbic acid per mg. Total antioxidant activity was tested using the phosphomolybdenum method and the absorbance was measured at 695 nm. The results are stated as one microgram of ascorbic acid is equivalent to one microgram of the test sample. Positive and negative controls were ascorbic acid and DMSO, respectively.[49]

2.13. Statistical analysis

Mean and standard deviation (SD) were calculated after repeating each of the quantifications thrice. One-tailed Student's *t*-test using SPSS Statistics 21 was used to analyze the data. P values < 0.05 were regarded as the level of significance to establish the significant differences between the groups.

3. Results and discussion

3.1. Characterization of Fe$_3$O$_4$@PPE nanoparticles

The biologically active molecules in the plant extract that are responsible for the formation of Fe$_3$O$_4$@PPE NPs were investigated using Fourier transform infrared spectroscopy (FTIR). A comparative FTIR analysis of pomegranate fruit peel extract and Fe$_3$O$_4$@PPE NPs was carried out. The results are presented in Fig. 3. A broadband peak at 3293 cm^{-1} in the FTIR spectrum of the pomegranate peel extract (PPE) shifted to 3195 cm^{-1} in the spectrum of Fe$_3$O$_4$@PPE, indicating the interaction of the polyphenolic –OH group of the peel extract with the functional group of Fe$_3$O$_4$@PPE nanoparticles *via* hydrogen bonding. The aliphatic C–H stretching peak observed around 2923 cm^{-1} in the PPE spectrum is weaker and shifts to 3055 cm^{-1} in the IR spectrum of Fe$_3$O$_4$@PPE, which is attributed to the binding of the C–H group to the Fe$_3$O$_4$@PPE nanoparticle surface. The appearance of vibrational peaks at 1712 and 1609 cm^{-1} in the PPE spectrum corresponded to the carbonyl functional groups, which appeared at 1627 cm^{-1} in the IR spectrum of Fe$_3$O$_4$@PPE, suggesting slight structural changes in the organic molecules on the surfaces of Fe$_3$O$_4$@PPE nanoparticles. The peak appeared at 1445 cm^{-1} in the PPE spectrum due to the vibrational stretching modes of the C=C bonds in the aromatic ring, which shifted to 1433 cm^{-1} in the IR spectrum of Fe$_3$O$_4$@PPE,
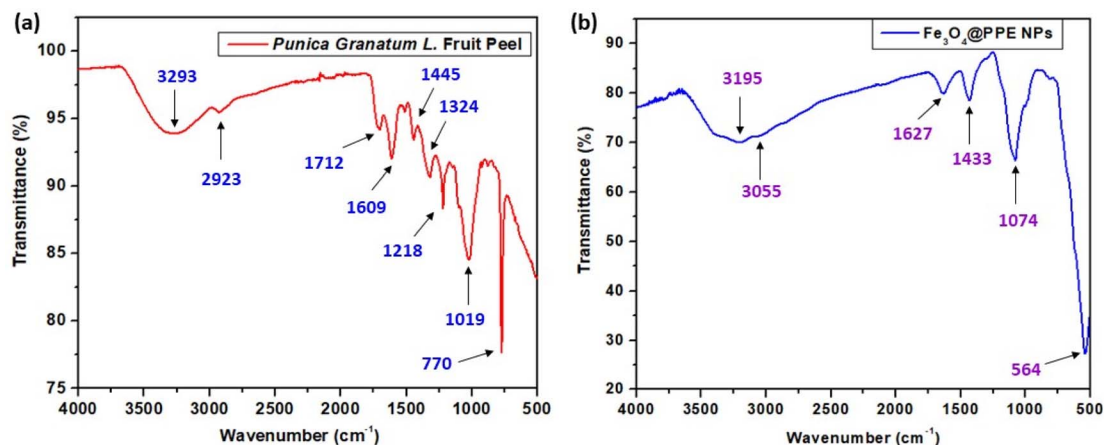
Fig. 3 FTIR spectra of (a) *Punica granatum* L. fruit peel extract and (b) Fe₃O₄@PPE NPs.

reflecting differences in the surface functionalization and C=C group interactions with the Fe_3O_4@PPE nanoparticles. Other peaks observed at 1324 and 1218 cm^{-1} in the PPE spectrum correspond to vibrational stretching modes of amino acid residues. The peaks presented at 1019 and 770 cm^{-1} are related to the tensile vibration of the C–O–C bond and aromatic C–H bending band in the FTIR spectrum of the pomegranate fruit peel extract. The presence of an additional peak at 564 cm^{-1} in Fe_3O_4@PPE, which is not present in the IR spectrum of pomegranate fruit peel extract, is attributed to the Fe–O bond.[50] On the other hand, the IR bands at 3195, 3055, 1627, 1433, and 1074 cm^{-1} in the Fe_3O_4@PPE NPs confirmed the presence of similar biomolecules in the iron oxide nanoparticles. This observation indicated the stabilization and encapsulation of Fe_3O_4 nanoparticles by the phytochemicals present in the pomegranate fruit peel extract.

Fig. 4 shows the X-ray diffraction (XRD) patterns of the *Punica granatum* L. fruit peel extract, biosynthesized Fe_3O_4@-PPE nanoparticles, and Fe_3O_4 nanoparticles without peel extract. XRD diffraction peaks of the Fe_3O_4@PPE nanoparticles appeared at $2\theta = 31.1°$ (2 2 0), 35.3° (3 1 1), 43.5° (4 0 0), and

63.3° (4 4 0), and are attributed to the crystalline character of Fe_3O_4 nanoparticles. These diffraction peaks are almost identical to the peaks of Fe_3O_4 nanoparticles without *Punica granatum* L. fruit peel extract. The diffraction patterns were also well matched with reported data.[51] The appearance of extra peaks in the XRD spectra of Fe_3O_4@PPE could be due to the crystallization of other biomolecules present in the *Punica granatum* L. fruit peel extract on the surfaces of the Fe_3O_4 nanoparticles. These findings indicate the successful encapsulation of Fe_3O_4@PPE NPs by the biomolecules present in the peel extract of pomegranate fruit. Similar observations were also noted with the previously reported methods for the synthesis of Fe_3O_4NPs@*Tridax procumbens* leaf extract,[52] Zn NPs@*Ziziphora clinopodioides* leaf extract,[53] and Ag NPs@*Areca catechu* leaf extract.[54]

Scanning electron microscopic images were recorded to establish the shape and morphological features of the Fe_3-O_4@PPE nanocatalyst. As shown in Fig. 5a, the morphology of the nanocatalyst is near-spherical. Energy dispersive X-ray spectroscopy (EDX) analysis offers information on the basic elemental composition of the biosynthesized Fe_3O_4@PPE nanocatalyst (Fig. 5b). EDX characterization reveals the absorption of a strong Fe signal along with other elements that might originate from the biomolecules present in the PPE plant extract. The synthesized nanocatalyst contains elements of carbon, oxygen, sulphur, and iron. The EDX spectra also exhibit signals at around 0.8, 6.4, and 7.1 keV, which are ascribed to the binding energies of iron,[55] confirming the synthesis of Fe_3-O_4@PPE nanocatalyst. The presence of other elements (C, O, and S) further indicated the successful formation of Fe_3O_4 NPs through the capping of the phytochemicals present in the PPE plant extract. Furthermore, the spatial distribution of each element was demonstrated by elemental mapping, which suggested that the C, O, S, and Fe elements are well dispersed over the structure of the synthesized nanocatalyst (Fig. S1, see the SI). The morphology and particle size distribution histogram (Fig. 5c and d) of the biosynthesized Fe_3O_4@PPE were further evaluated by transmission electron microscopy (TEM). TEM micrographs revealed that pomegranate peel extract-mediated
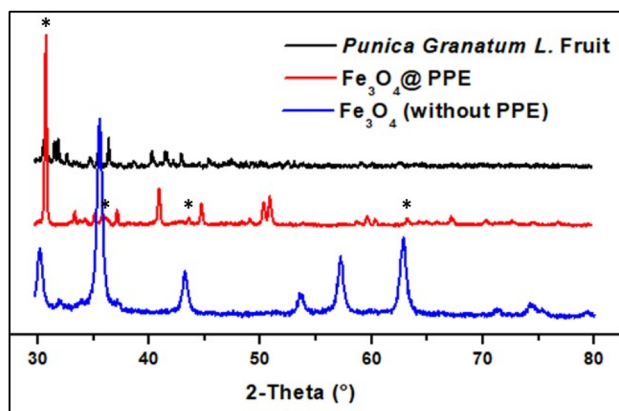

Fig. 4 X-ray diffraction (XRD) analysis of *Punica granatum* L. fruit peel extract and biosynthesized Fe_3O_4@PPE NPs.
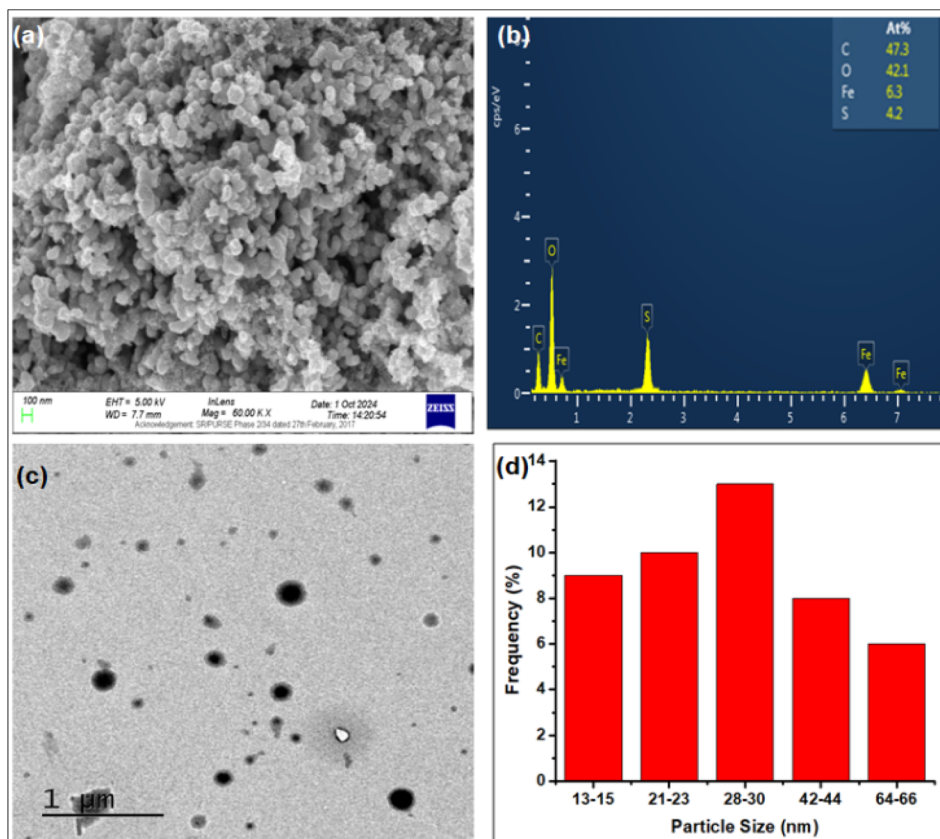
Fig. 5 (a) Scanning electron microscopic images, (b) energy dispersive X-ray spectra, (c) transmission electron microscopic images, and (d) particle size distribution histogram of the biosynthesized Fe_3O_4@PPE NPs.

iron oxide nanoparticles were mainly spherical in shape, with an average particle size of 21.4 nm, suggesting effective stabilization by the plant extract. Moreover, the particles exhibited good stability without further aggregation.

The dynamic light scattering (DLS) technique is one of the most widely used approaches to analyzing the hydrodynamic particle size and surface charge (ζ-potential) of nanomaterials (Fig. S2, see the SI). As displayed in Fig. S2, the *Z*-average

(hydrodynamic size) of the green biosynthesized Fe_3O_4@PPE NPs was 76.9 nm with a polydispersity index (PDI) value of 0.453, demonstrating that the Fe_3O_4@PPE NPs were reasonably monodispersed. The zeta potential showed a negative charge of -27.6 mV. The accumulation of metal core size, the size of the phytochemicals or biomolecules in the peel extract, and the electrical double layer between the nanoparticles all contribute to the hydrodynamic size of Fe_3O_4 nanoparticles. As a result, the
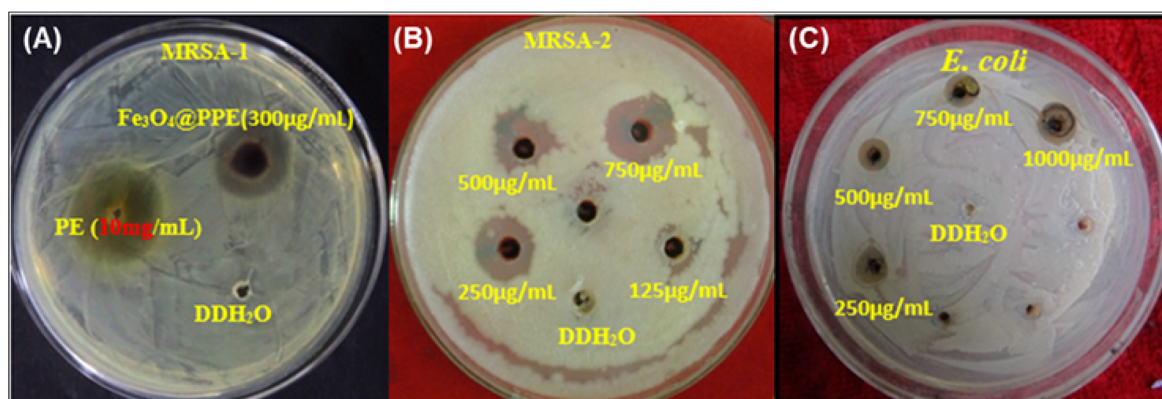

Fig. 6 Antibacterial activity of Fe_3O_4@PPE NPs against methicillin-resistant *Staphylococcus aureus* (MRSA1) (A and B) and *Escherichia coli* (C), which were grown on Mueller–Hinton agar plates at 37 °C. Distilled water and plant extract were used as negative and positive controls, respectively.

© 2025 The Author(s). Published by the Royal Society of Chemistry

average size of the biosynthesized Fe_3O_4@PPE NPs measured by DLS analysis is greater than that measured by macroscopic analysis (TEM). The negative zeta potential value (-27.6 mV) of the biosynthesized Fe_3O_4@PPE NPs indicates that the negatively charged functional groups of the biomolecules in the peel extract play an important role in determining the stability of the biosynthesized Fe_3O_4 nanoparticles.

3.2. Antibacterial activity of the biosynthesized Fe_3O_4@PPE nanoparticles

The continuous evolution of different strains of bacteria possessing multiple drug resistant properties in hospitals as well as in community settings has driven researchers to upgrade the synthesis of new types of antimicrobials.[12–15] Several studies have established the role of iron nanoparticles as an antibacterial agent, but intensive studies on the antibacterial activity of iron oxide nanoparticles are still needed.[16–19] The antimicrobial

Fig. 7 Zone of inhibition (mm) produced by Fe_3O_4@PPE NPs against methicillin-resistant *Staphylococcus aureus* (MRSA1 and MRSA2) and *Escherichia coli*. Values were expressed as mean $\pm$ SD.

Fig. 8 Zone of inhibition (mm) produced by Fe_3O_4@PPE NPs against *Staphylococcus aureus* (MRSA1 and MRSA2) and *Escherichia coli* at different concentrations of Fe_3O_4@PPE NPs (μg mL^{-1}). Values were expressed as mean $\pm$ SD.

activities of our biosynthesized Fe_3O_4@PPE nanoparticles with concentrations of 250, 500, 750 and 1000 μg mL^{-1} were tested against two methicillin-resistant *Staphylococcus aureus* isolates (MRSA1 and MRSA2), obtained from post-operative wounds,[42] and *Escherichia coli*, using the agar well diffusion method. The NPs showed antimicrobial activities against the target strains in a concentration dependent manner (Fig. 6–8). The antimicrobial properties of iron nanoparticles against *S. aureus* and *E. coli* were reported by Chatterjee *et al.*[18]

3.3. MIC and MBC values of the biosynthesized Fe_3O_4@PPE nanoparticles

The MIC values of the biosynthesized Fe_3O_4@PPE nanoparticles were 125 μg mL^{-1} to 250 μg mL^{-1}. The MIC was 150 μg mL^{-1} against MRSA1 strain and 125 μg mL^{-1} against MRSA2 (*Staphylococcus aureus* isolates). The MIC value against *Escherichia coli* was 250 μg mL^{-1}. On the other hand, MRSA1 and MRSA2 strains of *Staphylococcus aureus* showed MBC values of 250–300 μg mL^{-1}, while an MBC value of 500 μg mL^{-1} was recorded against *Escherichia coli* (Table S1, see the SI). Furthermore, the MIC and MBC values of the biosynthesized Fe_3O_4@PPE nanoparticles (125–150 μg mL^{-1} and 250–300 μg mL^{-1}, respectively) against *Staphylococcus aureus* were lower than the MIC and MBC values against *Escherichia coli* (250 μg mL^{-1} and 500 μg mL^{-1}, respectively). This was also reported by Thukkaram *et al.*[56] Moreover, the biosynthesized Fe_3O_4@PPE nanoparticles used in our study exhibited zones of inhibition for *Staphylococcus aureus* of 17.5 $\pm$ 0.48 mm to 21.5 $\pm$ 0.62 mm, whereas the inhibition zone for *Escherichia coli* was 13.5 $\pm$ 0.49 mm. The antibacterial activities of Fe_3O_4 NPs might involve the interaction between iron oxide nanoparticles (positively charged) and pathogenic bacteria (negatively charged), and the generation of ROS.[57,58] In addition, the outer membrane of Gram-negative bacteria serves as an obstacles to nanoparticle penetration and storage, and proteins associated with the membrane developing efflux pumps that effectively remove biocides and antibiotics.[59] A plausible mechanism of antibacterial activity of Fe_3O_4@PPE nanoparticles is shown in Fig. 9.

3.4. Antibiofilm activity of the biosynthesized Fe_3O_4@PPE nanoparticles

Advent of methicillin-resistant *Staphylococcus aureus* bacteria and their biofilm formation on medical devices remain as major problems.[12–15] In the present study, biofilm formation by MRSA1 and MRSA2 *Staphylococcus aureus* strains was found to be reduced significantly ($p < 0.05$) after treatment with the biosynthesized Fe_3O_4@PPE nanoparticles (Fig. 10). Previous studies suggest that biofilm formation might be reduced due to the inhibition of bacterial attachment to the glass surface.[57,59] Moreover, Fe_3O_4 NPs might exhibit antibiofilm activity through bactericidal activities involving the interaction between the iron oxide nanoparticles (positively charged) and pathogenic bacteria (negatively charged), and by the generation of ROS.[57,58] Besides this, the biosynthesized Fe_3O_4@PPE nanoparticles might be adhered to the negatively charged surface of the biofilm by electrostatic interactions and damage the biofilm,
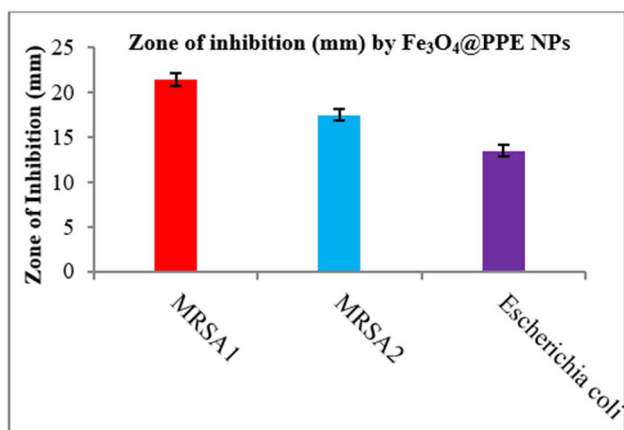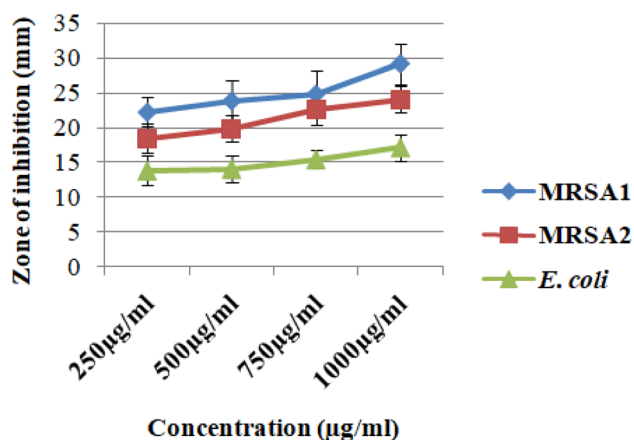
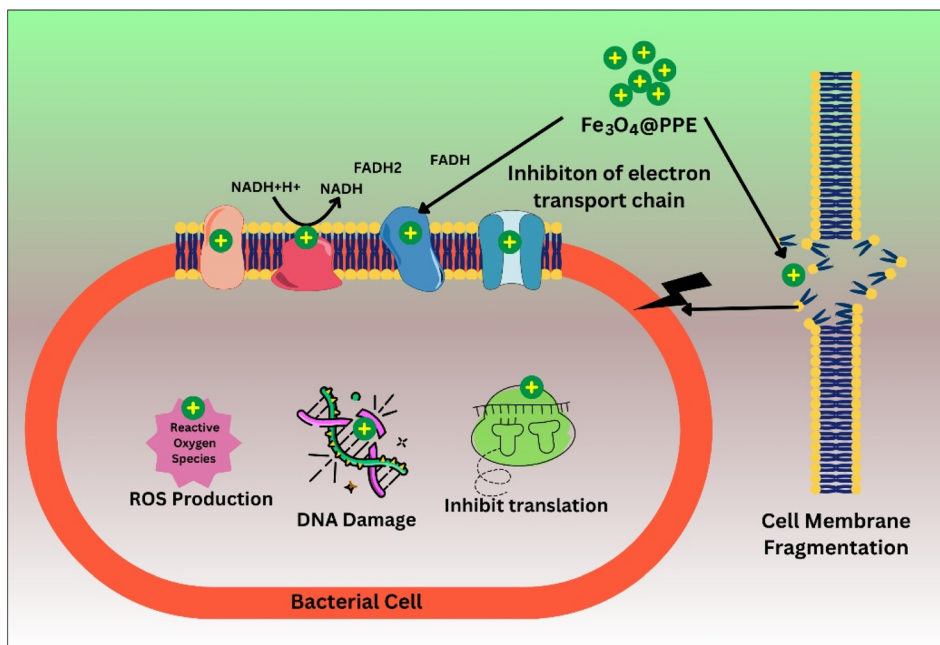**Fig. 9** Plausible mechanism for the antibacterial activity of the Fe_3O_4@PPE nanoparticles.

which leads to bacterial death within the biofilm.[58,60] Similar observations regarding the antibiofilm activity of the biosynthesized Fe_3O_4@PPE nanoparticles were also shown in other studies.[16–19] This was also consistent with the observations reported by Wang *et al.*[58] and Abdulla *et al.*[60] Thus, all the results suggest that the biosynthesized Fe_3O_4@PPE nanoparticles can be used against MRSA (Gram-positive) and Gram-negative bacteria, and they could also effectively inhibit chronic infections by reducing biofilm formation.[13] A schematic of the

mechanism of antibiofilm activity of Fe_3O_4@PPE nanoparticles is shown in Fig. 11.

3.5. Alpha-amylase inhibition by the biosynthesized Fe_3O_4@PPE nanoparticles

In the present study, it was found that alpha-amylase activity was effectively inhibited by the Fe_3O_4@PPE NPs, with maximum inhibition (50.89%) attained at 400 µg mL^{-1} (Fig. 12). The inhibition gradually decreased with decreasing concentration
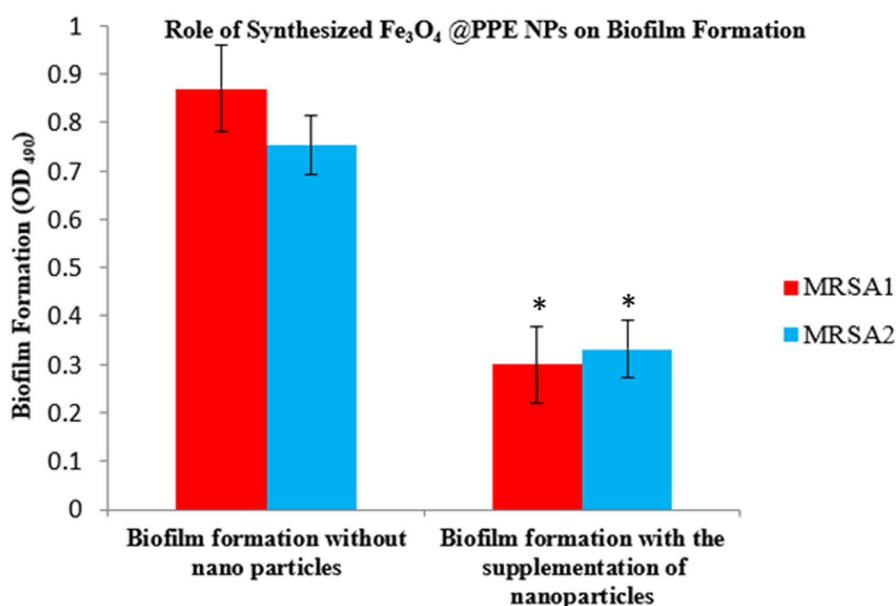

Fig. 10 Biofilm formation after supplementation with Fe_3O_4@PPE NPs against *Staphylococcus aureus* (MRSA1 and MRSA2). Values are expressed as mean ± SD. Student's *t*-test was performed. $P < 0.05$ was considered as the level of significance. "*" indicates significance.
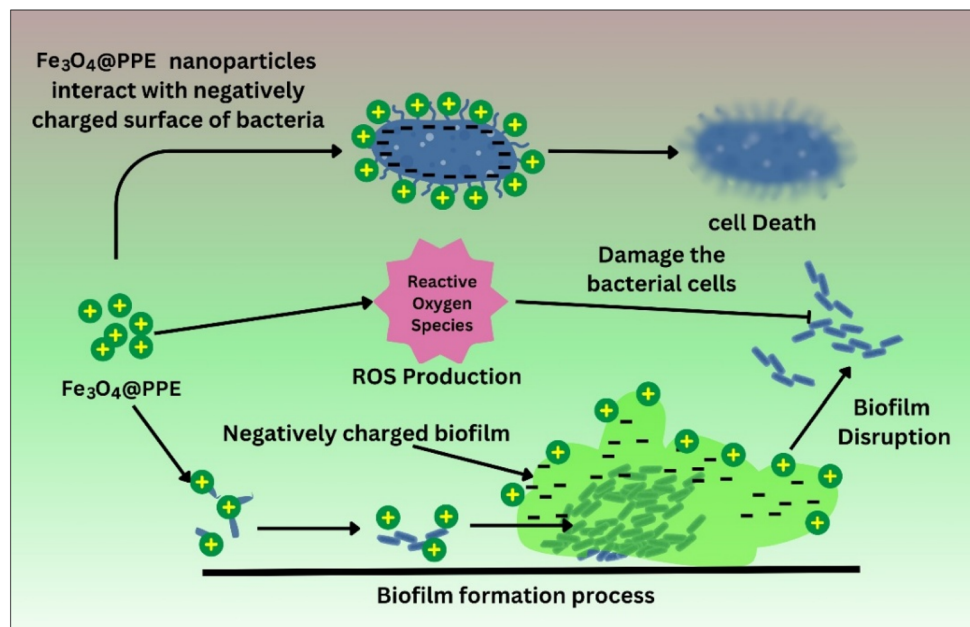
Fig. 11 Schematic of the mechanism of antibiofilm activity of the Fe_3O_4@PPE nanoparticles.

of Fe_3O_4@PPE NPs. Alpha amylase is reported to be involved in the breakdown of carbohydrates to glucose.[61] Thus, our biosynthesized Fe_3O_4@PPE NPs might reduce glucose levels by inhibiting alpha amylase and could be used as an antidiabetic agent.

3.6. Antioxidant activity of the biosynthesized Fe_3O_4@PPE nanoparticles

Studies on the antioxidant activities of the Fe_3O_4@PPE NPs (DPPH, TAC and TRP scavenging of free radicals), displayed in Fig. 13, revealed that the antioxidant activity increased with increasing concentration of Fe_3O_4@PPE NPs (1–200 μg mL^{-1}). The highest DPPH antioxidant potential was found to be 78.5% at 200 μg mL^{-1} for Fe_3O_4@PPE NPs. The maximum amount of the total antioxidants was 49.75% at 200 μg mL^{-1} (reducing

ability was evaluated ascorbic acid equivalent/milligram) for Fe_3O_4@PPE NPs. Total antioxidant capacity or TAC was used to confirm ROS scavenging property of the tested compounds. In the present study, the aqueous pomegranate fruit peel extract was used for reducing, oxidizing and capping. Phenolic compounds (high concentration) present in the peel of pomegranate are accepted as a natural resource for antioxidants with ROS scavenging properties.[20] These phenolic compounds are attached to the Fe_3O_4@PPE NPs in this study. TRP was also studied to determine the reductones, which are responsible for antioxidant activity by providing hydrogen atoms that might disrupt free radicals. The maximum reduction ability was 60.5% at 200 μg mL^{-1} for Fe_3O_4@PPE NPs. It can be speculated that several phenolic compounds or antioxidants present in the *Punica granatum* L. fruit peel extract might scavenge free radicals by donating hydrogen atoms or electrons present in their hydroxyl groups to the free radicals, thus generating DPPH–H
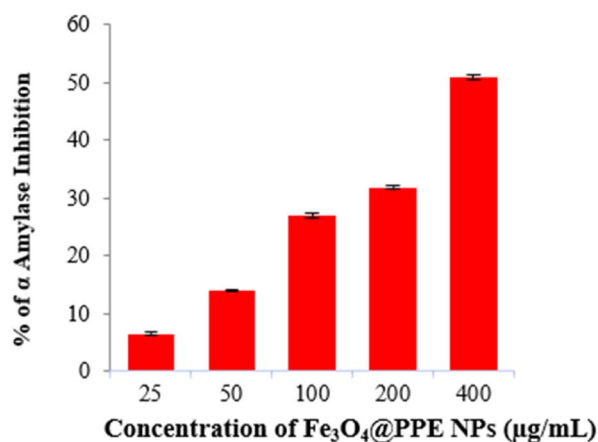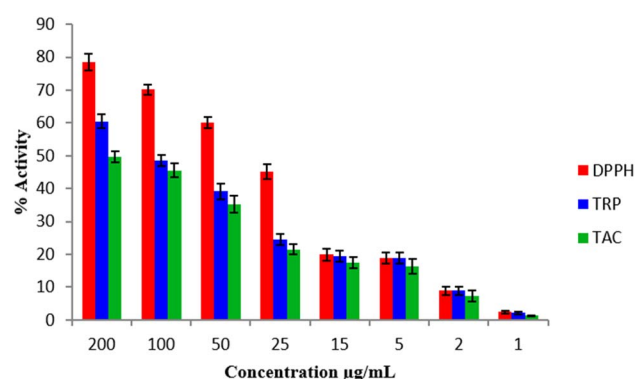

Fig. 12 Alpha amylase inhibition activity of Fe_3O_4@PPE NPs.

Fig. 13 Anti-oxidant activities of Fe_3O_4@PPE NPs.

by reducing DPPH free radicals. These observations are consistent with previous reports.[62]

A comparative analysis of Fe_3O_4@PPE NPs with previously reported antibacterial agents and the associated MIC, MBC and ZOI (zone of inhibition) values of the agents against bacteria are presented in Table S2, SI.
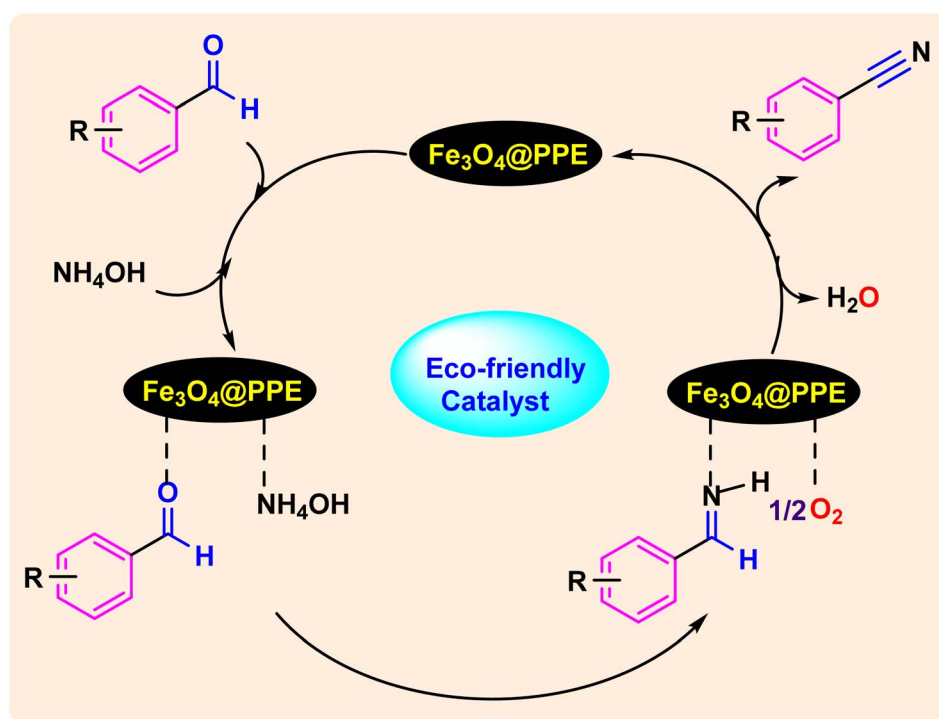
3.7. Catalytic ammoxidation of aromatic aldehydes to nitriles

The catalytic efficiency of the biosynthesized Fe_3O_4@PPE nanocatalyst was explored for the ammoxidation of benzaldehyde to benzonitrile in the presence of aqueous NH_3 as the source of nitrogen. The reaction was conducted at different temperatures and in different solvents, under an O_2 atmosphere, to establish the optimum conditions. The results are summarized in Table 1.

The reaction did not proceed in the absence of the catalyst, and the unreacted substrates were detected (Table 1, entry 1). This observation indicates that the Fe_3O_4@PPE provides the active sites for the catalytic ammoxidation of benzaldehyde to benzonitrile. Interestingly, the conversion of benzaldehyde increased to 47% when the reaction was performed in the presence of 2.4 wt% of Fe_3O_4@PPE nanocatalyst along with 700 μL of $NH_3 \cdot H_2O$ at 40 °C in EtOH medium (entry 2). Surprisingly, the conversion increased to 72% when the reaction was conducted using 3.2 wt% of Fe_3O_4@PPE nanocatalyst and 800 μL of $NH_3 \cdot H_2O$ at 60 °C in EtOH medium (entry 3). Improved conversion was achieved using 4.2 wt% of Fe_3O_4@PPE nanocatalyst under an O_2 atmosphere (entry 4). The yield of the reaction remained the same with a higher amount of Fe_3O_4@PPE nanocatalyst (entry 5). However, when the reaction was investigated under an argon atmosphere in the absence of O_2, no conversion of benzaldehyde was found in the reaction mixture (entry 6). This observation indicated the importance of atmospheric O_2 as the green oxidant during the catalytic ammoxidation of benzaldehyde to benzonitrile. However, when the reaction temperature was increased to 80 °C, the yield of the reaction was reduced to 68% (entry 7), indicating that, at higher temperatures, volatilization of NH_3 from the reaction mixture decreases the concentration of NH_3, which is unfavorable for the ammoxidation reaction. We next investigated the effect of different solvents in this reaction. When the reaction was studied using H_2O as solvent, the yield of the reaction decreased to 80% (entry 8), which could be due to the poor solubility of benzaldehyde in H_2O. With decreasing solvent polarity, the conversion of benzaldehyde decreased accordingly. n-Hexane led to an unsatisfactory yield of benzonitrile (entry 9), whereas CH_3CN, DMF and DMSO gave moderate reaction yields (entries 10–12). Therefore, EtOH was selected as the optimal solvent, and the conditions given in entry 4 were established as the optimized reaction conditions for subsequent investigations. The effective role of the EtOH solvent towards this ammoxidation reaction could be attributed to improved solubilization of the organic substrate and oxygen, as well as providing some stabilization of the imine intermediates through solvation. This stabilization may result in higher yields of the desired products.

Based on the above investigations and on literature reports,[63,64] a plausible reaction mechanism for this ammoxidation reaction is shown in Scheme 1. First, adsorption of aromatic aldehydes and NH_4OH takes place on the Fe_3O_4@PPE catalyst surface. The Fe_3O_4@PPE catalyst increases the electrophilicity of the aldehyde carbon, facilitating the immediate

Scheme 1 Plausible reaction mechanism for the ammoxidation of aromatic aldehydes using Fe_3O_4@PPE.

Table 2 Fe$_3$O$_4$@PPE-catalyzed ammoxidation of aromatic aldehydes to nitriles[a]

Entry	Substrate	Product	Time (h)	Yield (%)
1			24	91
2			24	87
3			24	85
4			24	84
5			24	89
6			24	87
7			24	81
8			26	78
9			24	82
10			24	80

[a] Reaction conditions: substrate (1.0 mmol), Fe$_3$O$_4$@PPE (40 mg), NH$_3$·H$_2$O (800 µL), EtOH (4 mL), under O$_2$ atmosphere, 60 °C. Yield of isolated and purified product.

formation of the imine intermediates by the reaction between the aldehyde and NH$_4$OH. Desorption of the corresponding nitrile products then takes place with the liberation of a H$_2$O molecule as the eco-friendly by-product from the imine intermediate in the presence of atmospheric O$_2$ and Fe$_3$O$_4$@PPE catalyst. This procedure demonstrates the usefulness of the Fe$_3$O$_4$@PPE catalyst in transforming aromatic aldehydes into beneficial nitriles. Consequently, applying this catalytic method not only increases the reaction rate, but also facilitates a more

RSC Advances

Paper

sustainable approach to chemical synthesis by reducing the formation of harmful byproducts.

We next investigated the catalytic efficiency of Fe_3O_4@PPE towards the synthesis of aryl nitriles by the ammoxidation of aromatic aldehydes under the optimal reaction conditions (Table 1, entry 4). The results are listed in Table 2. Various aromatic aldehydes, bearing both electron donating and electron withdrawing substituents, smoothly participated in this oxidative transformation. Benzaldehyde, as well as other aromatic aldehydes bearing electron-donating substituents, exhibited excellent catalytic reactivity and delivered the corresponding nitrile derivatives in good to high yields (Table 2, entries 1–4). Halogen-substituted aromatic aldehydes, such as 4-chlorobenzaldehyde and 4-bromobenzaldehyde, showed good conversion, and the corresponding nitriles were observed with 89% and 87% yield, respectively (entries 5 and 6).

The substrate conversion was poor in the case of hydroxyl-containing aromatic aldehydes, and the desired nitrile was obtained with 81% yield (entry 7). However, when the substituent was changed to an electron-withdrawing –NO_2 group, the yield of the corresponding nitrile decreased significantly even with a longer reaction time (entry 8). Interestingly, 4-acetylbenzaldehyde reacted efficiently and furnished the desired 4-acetylbenzonitrile with 82% yield (entry 9). This observation suggested that the ammoxidation reaction was highly selective for aldehydes. The present catalytic method was also successful for an electron-deficient heteroaromatic moiety containing a pyridine ring, and a satisfactory yield was observed

within 24 hours (entry 10). Thus, the Fe_3O_4@PPE shows good catalytic applicability for the ammoxidation of aromatic aldehydes to aryl nitriles.

From the perspective of "green and sustainable chemistry", the recyclability of the catalyst is essential.[9,65,66] Therefore, the recyclability of Fe_3O_4@PPE was examined using benzaldehyde (1 mmol), Fe_3O_4@PPE (40 mg), $NH_3\cdot H_2O$ (800 μL), and EtOH (4 mL), at 60 °C. All the catalytic runs were finished within 24 h under an O_2 atmosphere, and each catalytic cycle maintained a good yield without much reduction in reactivity (Fig. 14a). Furthermore, the recycled catalyst was also studied by SEM (Fig. 14b). The observations showed that the morphology of the spent Fe_3O_4@PPE catalyst almost remained same as that of the fresh Fe_3O_4@PPE catalyst. These investigations established that the developed catalyst exhibits good stability and high recyclability in the ammoxidation of benzaldehyde to benzonitrile.

A comparative study of the green biosynthesized Fe_3O_4@PPE-mediated ammoxidation of aldehydes with the earlier reported methods is presented in Table 3. All the reported synthetic approaches have their merits, but require an inert atmosphere,[67,69] high-temperature calcination,[67,69] and prolonged reaction time[67,69] during catalyst preparation, the use of organic solvents[68,69] or tedious product isolation procedures,[68,69] which limit their applicability from a green perspective. Therefore, in addition to being an economically efficient protocol, the present Fe_3O_4@PPE-catalyzed ammoxidation reaction, from the catalyst synthesis to the product separation in the presence of ethanol as a green reaction medium, is
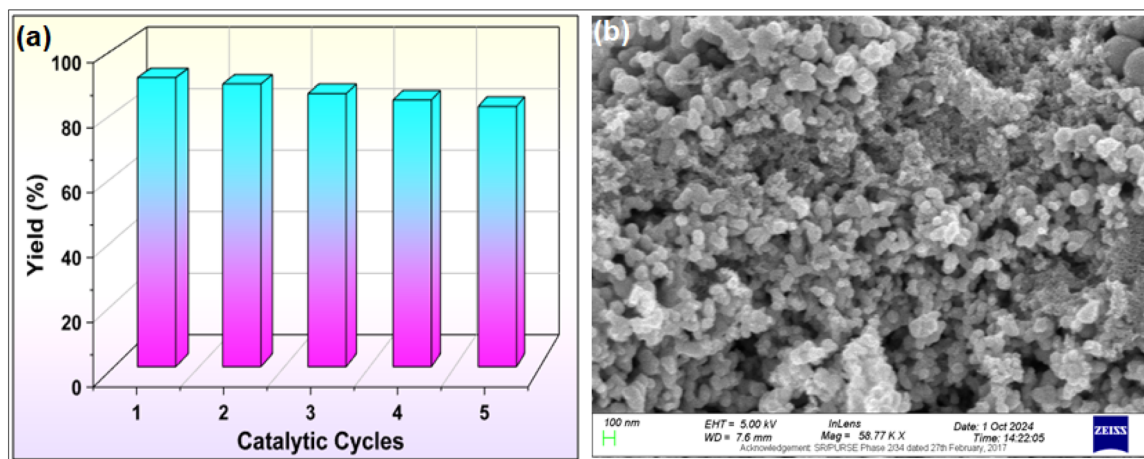

Fig. 14 (a) Recyclability test. (b) SEM image of the recycled Fe_3O_4@PPE catalyst.

Table 3 Comparison of the catalytic efficiency of Fe_3O_4@PPE with those of the previously reported catalysts for the ammoxidation of benzaldehyde

Entry	Catalyst	Nitrogen source	Solvent	Temp. (°C)/time (h)	Yield[a]/conversion (%)[b]	Ref.
1	Fe_2O_3@NC-800	$NH_3\cdot H_2O$	EtOH	60/24	99[a]	67
2	Fe/NC	$NH_3\cdot H_2O$	Bu_4NPF_6/MeCN	RT/24	83[b]	68
3	Co@CN-800	$(NH_4)_2CO_3$	DMSO	120/8	100[b]	69
4	Fe_3O_4@PPE	$NH_3\cdot H_2O$	EtOH	60/24	91[a]	This work

[a] Yield (%) of the reaction. [b] Conversion (%) of the reaction.

practically very simple. Furthermore, the present Fe_3O_4@PPE mediated protocol exhibits a novel and utilitarian catalytic methodology for the synthesis of pharmaceutically important nitriles from the ammoxidation of aldehydes with the survival of various functional groups under eco-compatible reaction media in comparison to previously reported approaches.

4. Conclusion

In this work, an economically efficient, operationally simple, and eco-friendly approach was adopted to synthesize Fe_3O_4 nanoparticles using an aqueous peel extract of pomegranate fruit. The UV-vis spectrum of the biosynthesized Fe_3O_4@PPE NPs showed an absorption peak at 370 nm. The hydrodynamic size (76.87 nm), polydispersity index (0.453), and zeta potential (−26.7 mV) of the biosynthesized Fe_3O_4@PPE NPs were determined using dynamic light scattering (DLS). The spherical morphology was observed for Fe_3O_4@PPE NPs with an average particle size of 21.4 nm. The green biosynthesized Fe_3O_4@PPE NPs exhibited strong antibacterial activities against both Gram-positive (MRSA1 and MRSA2) and Gram-negative (*Escherichia coli*) bacteria. The MIC values of the biosynthesized Fe_3O_4@PPE NPs against methicillin-resistant *Staphylococcus aureus* strains (MRSA1 and MRSA2) and *E. coli* (Gram-negative) were 150 μg mL^{-1} and 125 μg mL^{-1}, and 250 μg mL^{-1}, respectively. On the other hand, the MBC values for MRSA1 and MRSA2 were 300 μg mL^{-1} and 250 μg mL^{-1}, respectively, and 500 μg mL^{-1} for *Escherichia coli*. Moreover, the biosynthesized Fe_3O_4@PPE NPs could also be effective in inhibiting chronic infections by reducing the biofilm formation. On the other hand, our biosynthesized Fe_3O_4@PPE NPs were able to lower glucose levels by inhibiting amylase activity, indicating their anti-diabetic potential (50.89% alpha-amylase inhibition at 400 μg mL^{-1}). Furthermore, the biosynthesized Fe_3O_4@PPE NPs were found to scavenge ROS (78.5% at 200 μg mL^{-1}), which demonstrates their anti-oxidant activity. The catalytic proficiency of the green biosynthesized Fe_3O_4@PPE NPs has been shown for the ammoxidation of aromatic aldehydes to aryl nitriles under an oxygen atmosphere. Remarkably, the catalyst was recycled in five consecutive runs and retained its good catalytic efficacy. Attractive features of this green synthetic route are the utilization of easily accessible starting materials, such as aldehydes and ammonia, and the use of atmospheric O_2 as an eco-friendly oxidant.

Conflicts of interest

The authors declare that they have no known competing financial interests or personal relationships that could have appeared to influence the work reported in this paper.

Data availability

The data supporting this article have been included as part of the SI. Supplementary information is available. See DOI: https://doi.org/10.1039/d5ra04814a.

Notes and references

1 C. Tanase, L. Berta, N. A. Coman, I. Rosca, A. Man, F. Toma, A. Mocan, L. Jakab-Farkas, D. Biro and A. Mare, *Antioxidants*, 2019, **459**, 8.

2 M. T. Nguyen and T. Yonezawa, *Sci. Technol. Adv. Mater.*, 2018, **19**, 883–898.

3 J. A. Darr, J. Zhang, N. M. Makwana and X. Weng, *Chem. Rev.*, 2017, **117**, 11125–11238.

4 L. Lee, C. Xiao, W. Huang and Y. Zhao, *New J. Chem.*, 2015, **39**, 2459–2466.

5 A. V. Nikam, B. L. V. Prasad and A. A. Kulkarni, *CrystEngComm*, 2018, **20**, 5091–5107.

6 A. LaGrow, M. O. Besenhard, A. Hodzic, A. Sergides, L. K. Bogart, A. Gavriilidis and N. T. K. Thanh, *Nanoscale*, 2019, **11**, 6620–6628.

7 K. Wang, L. Yang, W. Zhao, L. Cao, Z. Sun and F. Zhang, *Green Chem.*, 2017, **19**, 1949–1957.

8 J. S. Qin, S. Yuan, C. Lollar, J. Pang, A. Alsalme and H. C. Zhou, *Chem. Commun.*, 2018, **54**, 4231–4249.

9 A. K. Das, S. Ali, A. Misra, S. Islam, B. Kar, S. Biswas, G. Ghatak, D. Mal, M. Shit, M. Dolai and A. Das, *Appl. Organomet. Chem.*, 2025, **39**, e7796.

10 R. J. Turner, *J. Microb. Biotechnol.*, 2017, 1062–1065.

11 J. Hasan, R. J. Crawford and E. P. Ivanova, *J. Microb. Biotechnol.*, 2013, **31**, 295–304.

12 J. A. Lemire, J. J. Harrison and R. J. Turner, *Nat. Rev. Microbiol.*, 2013, **11**, 371–384.

13 J. W. Costerton, P. S. Stewart and E. P. Greenberg, *Science*, 1999, **284**, 1318–1322.

14 M. Otto, Staphylococcal biofilms, *Bacterial Biofilms*, 2008, pp. 207–228, DOI: 10.1007/978-3-540-75418-3.

15 L. Hall-Stoodley, J. W. Costerton and P. Stoodley, *Nat. Rev. Microbiol.*, 2004, **2**, 95–108.

16 N. Tran, A. Mir, D. Mallik, A. Sinha, S. Nayar and T. J. Webster, *Int. J. Nanomed.*, 2010, **5**, 277.

17 S. L. Iconaru, A. M. Prodan, P. Le Coustumer and D. Predoi, *J. Chem.*, 2013, **2013**, 412079, DOI: 10.1155/2013/412079.

18 S. Chatterjee, A. Bandyopadhyay and K. Sarkar, *J. Nanobiotechnol.*, 2011, **9**, 1–7.

19 D. M. Salem, M. M. Ismail and H. R. Tadros, *Egypt. J. Aquat. Res.*, 2020, **46**, 333–339.

20 B. Singh, J. P. Singh, A. Kaur and N. Singh, *Food Chem.*, 2018, **261**, 75–86.

21 B. N. Patra, A. K. Das, S. Misra, P. P. Jana, P. Brandao, M. Afzal, A. Alarifi, T. Saha, D. Bera, S. Halder, D. Mal and N. Sepay, *J. Mol. Struct.*, 2024, **1300**, 137229.

22 A. K. Das and K. Sarkar, *New J. Chem.*, 2025, **49**, 12898–12930.

23 A. Pramanik, A. K. Das, S. Bhar and A. Ghatak, *ChemistrySelect*, 2025, **10**, e202500035.

24 D. Saha, A. K. Das, M. Raish and N. Sepay, *J. Mol. Struct.*, 2025, **1329**, 141363.

25 S. Nandy, A. Ghatak, A. K. Das and S. Bhar, *Synlett*, 2018, **29**, 2208–2212.

26 R. C. Larock, in *Comprehensive Organic Transformations: A Guide to Functional Group Preparations*, Wiley-VCH, Weinheim, Germany, 1989, pp. 819–995.

27 A. M. Sweeney, P. Grosche, D. Ellis, K. Combrink, P. Erbel, N. Hughes, F. Sirockin, S. Melkko, A. Bernardi, P. Ramage, N. Jarousse and E. Altmann, *ACS Med. Chem. Lett.*, 2014, **5**, 937–941.

28 T. Sandmeyer, *Chem. Ber.*, 1885, **18**, 1492–1496.

29 K. W. Rosenmund and E. Struck, *Chem. Ber.*, 1919, **2**, 1749–1756.

30 C. Qin and N. Jiao, *J. Am. Chem. Soc.*, 2010, **132**, 15893–15895.

31 D. D. Beattie, T. Schareina and M. Beller, *Org. Biomol. Chem.*, 2017, **15**, 4291–4294.

32 G. Wang, X. Xie, W. Xu and Y. Liu, *Org. Chem. Front.*, 2019, **6**, 2037–2042.

33 D. Tsuchisya, Y. Kawagoe, K. Moriyama and H. Togo, *Org. Lett.*, 2013, **15**, 4194–4197.

34 W. Zhou, J. Xu, L. Zhang and N. Jiao, *Org. Lett.*, 2010, **12**, 2888–2891.

35 C. B. Kelly, K. M. Lambert, M. A. Mercadante, J. M. Ovian, W. F. Bailey and N. E. Leadbeater, *Angew. Chem., Int. Ed.*, 2015, **54**, 4241–4245.

36 A. Sadhukhan, B. N. Patra, T. Maity, A. K. Das, C. K. Ghosh, P. Brandao, D. M. Gil, D. Bera, C. Roy Choudhury, P. K. Bhaumik, D. Mal and A. Frontera, *Eur. J. Inorg. Chem.*, 2024, **27**, e202400459.

37 A. Das and A. K. Das, *New J. Chem.*, 2023, **47**, 5347–5355.

38 A. K. Das, S. Nandy and S. Bhar, *RSC Adv.*, 2022, **12**, 4605–4614.

39 A. K. Das, N. Sepay, S. Nandy, A. Ghatak and S. Bhar, *Tetrahedron Lett.*, 2020, **61**, 152231.

40 S. Nandy, A. K. Das and S. Bhar, *Synth. Commun.*, 2020, **50**, 3326–3336.

41 A. K. Das, S. Nandy and S. Bhar, *Appl. Organomet. Chem.*, 2021, **35**, e6282.

42 S. Biswas and K. Pal, *Int. J. Pharm. Biol. Sci.*, 2017, **7**, 241–247.

43 A. W. Bauer, W. M. Kirby, J. C. Sherris and M. Turck, *Am. J. Clin. Pathol.*, 1966, **45**, 493.

44 P. A. Wayne and Clinical and Laboratory Standards Institute (CLSI), in *Performance Standards for Antimicrobial Susceptibility Testing*, CLSI, 26th edn, 2016.

45 M. Khatami and S. Pourseyedi, *IET Nanobiotechnol.*, 2015, **9**, 184–190.

46 C. Heilmann, C. Gerke, F. Perdreau-Remington and F. Gotz, *Infect. Immun.*, 1996, **64**, 277–282.

47 A. T. Khalil, M. Ovais, I. Ullah, M. Ali, Z. K. Shinwari, D. Hassan and M. Maaza, *Artif. Cells, Nanomed. Biotechnol.*, 2018, **46**, 838–852.

48 A. Baqi, R. B. Tareen, A. Mengal, N. Khan, F. Behlil, A. K. K. Achakzai and M. Faheem, *Pure Appl. Biol.*, 2018, **7**, 296–308.

49 S. Satpathy, A. Patra, B. Ahirwar and M. D. Hussain, *Artif. Cells, Nanomed. Biotechnol.*, 2018, **3**, 71–85.

50 R. A. Sobh, H. E. Nasr and W. M. Sabry, *Egypt. J. Chem.*, 2020, **63**, 507–514.

51 M. Qi, K. Zhang, S. Li, J. Wu, C. Pham-Huy, X. Diao and H. He, *New J. Chem.*, 2016, **40**, 4480–4491.

52 M. Senthil and C. Ramesh, *Dig. J. Nanomater. Biostruct.*, 2012, **7**, 1655–1660.

53 B. Mahdavi, S. Saneei, M. Qorbani, M. Zhaleh, A. Zangeneh, M. M. Zangeneh, E. Pirabbasi, N. Abbasi and H. Ghaneialvar, *Appl. Organomet. Chem.*, 2019, e5164.

54 G. Shruthi, K. ShivaPrasad, T. P. Vinod, V. Balamurugan and C. Shivamallu, *ChemistrySelect*, 2017, **2**, 10354–10359.

55 P. Veerakumar, I. P. Muthuselvam, C. T. Hung, K. C. Lin, F. C. Chou and S. B. Liu, *ACS Sustainable Chem. Eng.*, 2016, **4**, 6772–6782.

56 M. Thukkaram, S. Sitaram, S. K. Kannaiyan and G. Subbiahdoss, *Int. J. Biomater.*, 2014, **2014**, 716080, DOI: 10.1155/2014/716080.

57 Y. T. Prabhu, K. V. Rao, B. S. Kumari, V. S. S. Kumar and T. Pavani, *Int. Nano Lett.*, 2015, **2**, 85–92.

58 X. Wang, A. Deng, W. Cao, Q. Li, L. Wang, J. Zhou, B. Hu and X. Xing, *J. Mater. Sci.*, 2018, **9**, 6433–6449.

59 A. Mahamoud, J. Chevalier, S. Alibert-Franco, W. V. Kern and J. M. Pagès, *J. Antimicrob. Chemother.*, 2007, **59**, 1223–1229.

60 A. Abdulla, A. A. ALthahab, T. A. Abed, R. K. Mahdi and S. Fadhil, *Int. J. Curr. Res. Acad. Rev.*, 2015, **3**, 128–134.

61 G. Yao, F. M. Sebisubi, L. Y. C. Voo, C. C. Ho, G. T. Tan and L. C. Chang, *J. Braz. Chem. Soc.*, 2011, **22**, 1125–1129.

62 B. A. Abbasi, J. Iqbal, T. Mahmood, A. Qyyum and S. Kanwal, *Appl. Organomet. Chem.*, 2019, **33**, e4947.

63 T. Senthamarai, V. G. Chandrashekhar, N. Rockstroh, J. Rabeah, S. Bartling, R. V. Jagadeesh and M. Beller, *Chem*, 2022, **8**, 508–531.

64 H. Zhao, X. Sun, D. Xu, Q. Zhu, Y. Zhu and Z. Dong, *J. Colloid Interface Sci.*, 2020, **565**, 177–185.

65 A. Das, D. Chavda, M. Manna and A. K. Das, *New J. Chem.*, 2024, **48**, 18249–18260.

66 A. Ghatak, A. Pramanik, A. K. Das and S. Bhar, *Tetrahedron*, 2022, **127**, 133090.

67 W. D. Wang, F. Wang, Y. Chang and Z. Dong, *Mol. Catal.*, 2021, **499**, 111293.

68 C. Wang, J. Li, T. Shao, D. Zhang, Y. Mai, Y. Li, F. Besenbacher, H. Niemantsverdriet, F. Rosei, J. Zhong and R. Su, *Angew. Chem., Int. Ed.*, 2023, **62**, e202313313.

69 L. Pan, W. Fu, L. Zhang, S. Wang and T. Tang, *Mol. Catal.*, 2022, **518**, 112087.